OCT 1992

UM-AC-92-12

MAGNETOHYDRODYNAMIC WAVE PROPAGATION IN 1-D NONHOMOGENEOUS, SELFGRAVATATING CLOUDS

Marco Fatuzzo and Fred C. Adams
Physics Department, University of Michigan
Michigan U.

to appear in The Astrophysical Journal, July 1993

UM AC 92-12

MAGNETOHYDRODYNAMIC WAVE PROPAGATION IN 1-D NONHOMOGENEOUS, SELF-GRAVITATING CLOUDS

Marco Fatuzzo[1] and **Fred C. Adams**

Physics Department, University of Michigan
Ann Arbor, MI 48109

26 October, 1992
submitted to The Astrophysical Journal

ABSTRACT

We study the propagation of magnetohydrodynamic (MHD) waves through nonhomogeneous, self-gravitating, magnetic media representative of molecular cloud environments and focus on the issues of cloud support and line profiles. Since the general treatment of this topic is burdened by a complex mathematical formalism, we consider simplifying geometries which yield analytical solutions in the linear wave limit. In particular, we study both magnetoacoustic and Alfvén wave propagation along the density gradient in a one-dimensional slab. Of specific relevance to molecular clouds, we find that the back-reaction of the Alfvén waves can provide a pressure along the direction of the magnetic field lines; this pressure can help support a density enhancement against gravitational collapse. Furthermore, we find that the velocity amplitudes of these waves increase as the density decreases, in rough agreement with observational estimates of line-width vs density relations.

Subject headings: hydromagnetics – wave motions – interstellar: molecules – stars: formation

[1] Compton GRO Fellow.

1. INTRODUCTION

The observed inefficiency of star formation suggests that molecular clouds cannot be collapsing on free-fall timescales (Zuckerman & Palmer 1974). This point is further strengthened by the analysis of a cloud within the Taurus complex, which indicates no evidence for global collapse (Murphy & Myers 1985). In contrast, the thermal Jean's mass in a typical cloud is generally quite small compared to the actual physical mass, and consequently, thermal pressure can provide support against gravitational collapse only at the smallest scales (e.g., molecular cloud cores). On the other hand, magnetic fields with strengths of $\sim 10 - 100\mu$G are now observed in molecular cloud environments (see, e.g., the reviews by Heiles 1987; Kazés et al. 1987, and references therein; Goodman et al. 1989); thus, magnetic pressure is capable of providing the inferred large scale support (Chandrasekhar & Fermi 1953; Mestel 1965; Strittmatter 1966; Spitzer 1968; Mouschovias & Spitzer 1976; Mouschovias 1976).

A shortcoming of the magnetic support paradigm is its inability to provide a static pressure along the field line direction. Since magnetic field lines in molecular clouds seem to be extremely well ordered (Schwarz et al. 1986; Goodman 1990), a static cloud should therefore exhibit a sheet-like morphology. Although such structure is sometimes observed, it is not a general feature of cloud complexes. This finding suggests that the underlying magnetic fields are dynamic. Indeed, it has been noted that the "observed" turbulence, which has itself been suggested as a possible support mechanism (Larson 1981; Bonnazzola et al. 1987), will excite a spectrum of magnetohydrodynamic (MHD) waves (Arons & Max 1975; Elmegreen 1985; Falgorne & Puget 1986) whose outward propagation may provide a pressure contribution along the direction of the field lines (Dewar 1970; Shu, Adams, & Lizano 1987; Pudritz 1990). This mechanism is consistent with observed molecular line profiles (Falgorne & Puget 1986; Myers & Goodman 1988), whose widths imply supersonic (but subalfvénic) motion that would be highly dissipative in the absence of the fields.

The overall goal of this paper is to study MHD wave support in molecular clouds and to consider the relationship between these waves and the observed molecular line profiles. A complete treatment of this problem requires an understanding of wave propagation (and dissipation) in self-gravitating, *nonhomogeneous*, magnetic media. The nonhomegeneity of the medium is an important element because observed clouds exhibit highly nonlinear structure (e.g., Wood, Daughterty, & Myers 1992; Wiseman & Adams 1992; Houlahan & Scalo 1992) and because wave propagation through nonuniform media has not been well studied. Unfortunately, the presence of a gravitational potential along with a realistic nonhomogeneous medium makes a completely analytical treatment of linear wave propagation intractable for most geometries (we note that most previous studies have ignored both self-gravity and the nonhomogeneity of the background state). In this paper we present a special case where such a treatment can be carried out. In particular, we consider linear magnetohydrodynamic wave propagation in a slablike geometry for both magnetoacoustic and Alfvén waves. Since the damping rate of these waves is expected to be shorter than the cloud lifetime (Zweibel & Josafattson 1983), we include the dissipative effects of field-line diffusion through the neutral component. We point out, however, that other important dissipative mechanisms (such as the nonlinear processes discussed by Zweibel & Josafattson 1983) are not considered here. Although our results are relevant in many

different contexts, we focus on the specific issues of overall cloud support and line-width vs density relationships.

This paper is organized as follows. We present the general formalism for wave propagation through a nonhomogeneous, self-gravitating medium in §2. In §3, we consider a simplifying one dimensional geometry which lends itself to the analytical treatment of magnetoacoustic wave propagation; we also determine the wave-background interactions which may contribute to the magnetic support across the field lines. In §4, we present an analogous format to §3, but for a simplifying geometry which lends itself to the analytical treatment of Alfvén waves. We show that Alfvén waves can provide support along field lines. We compare our results to observations in §5, and conclude with a discussion in §6. As a final comment, we note that although the simplifications made in this calculation limit the interpretation of our results, they are warranted by the benefits of an analytical treatment. Furthermore, our results may be directly applicable to clouds or parts of clouds with sheet-like geometries.

2. GENERAL FORMALISM

In this section we present a general formalism for wave propagation through nonhomogeneous density distributions. We idealize the molecular cloud environment as a slightly ionized fluid threaded by a magnetic field. The electrons are ignored in the fluid dynamics since they are not as strongly coupled to the neutrals as the ions and since they represent a negligible fraction of the overall mass. The presence of the electrons only serves to maintain charge neutrality. The grains are also ignored in the fluid dynamics since their effect is minimal when the neutral number density $n \lesssim 10^4$ cm^{-3} (Nishi, Nakano, & Umebayashi 1991). However, grains do play an important role in the ionization balance, and are considered in this regard. We assume that flux-freezing fully couples the charged particles to the magnetic field, and consequently, that the neutral fluid is coupled (albeit indirectly) to the magnetic field through its interaction with the ion fluid. As long as the relative velocity between ions and neutrals is small ($\lesssim 10$ km s^{-1}), this interaction is dominated by Langevin scattering, which produces a force density exerted on the neutral fluid (by the ions) of the form

$$\mathbf{f}_{ni} = \gamma \rho \rho_i (\mathbf{v}_i - \mathbf{v}) \ , \tag{2.1}$$

where $\rho_{(i)}$ and $\mathbf{v}_{(i)}$ are the neutral (ion) mass density and velocity, respectively, and where

$$\gamma = 3.5 \times 10^{13} \mathrm{cm}^3 \mathrm{g}^{-1} \mathrm{s}^{-1} \tag{2.2}$$

(for further discussion, see Draine, Roberge, & Dalgarno 1983; Shu, Adams, & Lizano 1987; Shu 1992).

The dynamical equations for the ion and neutral fluids are

$$\rho \frac{\partial \mathbf{v}}{\partial t} + \rho (\mathbf{v} \cdot \nabla) \mathbf{v} = -\rho \nabla \Phi - \nabla p + \mathbf{f}_{ni} \ , \tag{2.3}$$

and

$$\rho_i \frac{\partial \mathbf{v}_i}{\partial t} + \rho_i (\mathbf{v}_i \cdot \nabla) \mathbf{v}_i = -\rho_i \nabla \Phi - \nabla p_i + \frac{(\nabla \times \mathbf{B}) \times \mathbf{B}}{4\pi} - \mathbf{f}_{ni} \ , \tag{2.4}$$

respectively, where $p_{(i)}$ is the neutral (ion) gas pressure, Φ is the gravitational potential, and $\mathbf{B}$ is the magnetic field. The minimal effects that ionization and recombination have on the dynamics are ignored. In the applicable limit that $\rho_i \ll \rho$, bulk MHD wave motion occurs only if the neutrals are well coupled to the ions. We therefore consider waves with frequencies ω lower than the neutral-ion collision frequency ($\gamma\rho_i$). Under these conditions, the first four terms in equation (2.4) are negligible, and the ion-neutral frictional force is balanced by the Lorentz force, i.e.,

$$\gamma\rho\rho_i(\mathbf{v}_i - \mathbf{v}) = \frac{(\nabla \times \mathbf{B}) \times \mathbf{B}}{4\pi} . \tag{2.5}$$

The physical meaning of equation (2.5) is that the Lorentz force drives the ions through the sea of neutrals. The equation of motion for the neutral fluid may therefore be expressed as

$$\rho\frac{\partial \mathbf{v}}{\partial t} + \rho(\mathbf{v} \cdot \nabla)\mathbf{v} = -\rho\nabla\Phi - a_s^2\nabla\rho + \frac{(\nabla \times \mathbf{B}) \times \mathbf{B}}{4\pi} , \tag{2.6}$$

where an isothermal equation of state $p = a_s^2\rho$ with constant sound speed a_s has been assumed. The effects of magnetic diffusion through the neutrals is represented in the dynamics equation through $\mathbf{B}$ via the magnetic induction equation

$$\frac{\partial \mathbf{B}}{\partial t} = \nabla \times (\mathbf{v} \times \mathbf{B}) + \nabla \times \left\{ \frac{[(\nabla \times \mathbf{B}) \times \mathbf{B}] \times \mathbf{B}}{4\pi\gamma\rho\rho_i} \right\} . \tag{2.7}$$

With $\nabla \cdot \mathbf{B} = 0$ as an initial condition, the neutral fluid is thus described by equations (2.6) and (2.7), the continuity equation

$$\frac{\partial \rho}{\partial t} + \nabla \cdot (\rho\mathbf{v}) = 0 , \tag{2.8}$$

and Poisson's equation

$$\nabla^2\Phi = 4\pi G\rho , \tag{2.9}$$

where we have neglected ionic inertia ($\rho_i \ll \rho$).

To close the system of equations, the ion mass density ρ_i must be specified. The ion population depends on the complex balance between the ionization rate of neutrals (through cosmic rays, etc.), the subsequent production of molecular and metal ions, and the ion-electron recombination in the presence of grains. However, a reasonable approximation for the ionic mass density in molecular cloud environments is given by

$$\rho_i = C\rho^{1/2} , \tag{2.10}$$

where

$$C = 3 \times 10^{-16}\mathrm{cm}^{-3/2}\mathrm{g}^{1/2} \tag{2.11}$$

(Elmegreen 1979). In the presence of perturbations leading to compression or rarefaction, equation (2.10) is valid only for perturbation timescales which are are much longer than the re-equilibration timescale. In contrast, if the re-equilibration timescale is long compared to

the perturbation timescale, the ratio of the perturbed to unperturbed ion density is equal to the ratio of the perturbed to unperturbed neutral density, and the fluid will be either overionized or underionized with respect to the corresponding equilibrium state.

The primary ionization process in molecular clouds is cosmic-ray ionization, resulting in the formation of complex molecular ions. Although these molecular ions rapidly neutralize via dissociative recombination, they also rapidly transfer charges with heavy metal atoms whose neutralization occurs via the slower radiative recombination process. As a result, metal ions dominate the ionic fluid (Oppenheimer & Dalgarno 1974; Elmegreen 1979). For neutral number densities larger than $n > 1$ cm^{-3}, most recombination of metals occurs on grains (see Fig. 1 in Elmegreen 1979). For typical cloud environments (i.e., $T = 10$ K, a metal depletion factor $\delta = 0.1$, an ionization rate $\zeta = 10^{-17}$ s^{-1}, grain radii of $a = 0.32$ μm, and 1 cm^{-3} $< n < 10^5$ cm^{-3}), the fraction of all grains that are charged with Q $= -1$ is $\gtrsim 0.9$ (see Table I in Elmegreen 1979). Assuming that the bulk velocity due to the wave motion has no effect on the metal-grain collision rate coefficient, we find that its value is given by

$$\alpha_{Eg}(Q=-1) = 2.6 \times 10^{-4}\ \mathrm{cm}^3\ \mathrm{s}^{-1} \left(\frac{T}{10\mathrm{K}}\right)^{-1/2} \left(\frac{a}{0.3\mu\mathrm{m}}\right) \left(\frac{m_E}{30 m_H}\right)^{-1/2}, \tag{2.12}$$

and the metal neutralizing timescale $\tau_N \sim 1/n_g \alpha_{Eg}$ is therefore approximately

$$\tau_N \sim 10^5\ \mathrm{yr} \left(\frac{n}{10^3 \mathrm{cm}^{-3}}\right)^{-1} \left(\frac{n_g/n}{10^{-12}}\right)^{-1} \left(\frac{T}{10\mathrm{K}}\right)^{1/2} \left(\frac{a}{0.3\mu\mathrm{m}}\right)^{-1} \left(\frac{m_E}{30 m_H}\right)^{1/2}, \tag{2.13}$$

where m_E is the metal ion mass, m_H is the hydrogen mass, and n_g is the grain number density. Since the unperturbed cloud is in charge equilibrium, the ionization rate must be equal to the recombination rate. The timescale required to re-equlibrate a perturbed system is therefore $\tau_{eq} \ll \tau_N$. In contrast, the MHD wave timescale is given by

$$\tau_{MHD} \approx 10^6\ \mathrm{yr} \left(\frac{\lambda}{1\mathrm{pc}}\right) \left(\frac{v_\alpha}{1\mathrm{km\ s}^{-1}}\right)^{-1}. \tag{2.14}$$

We therefore assume that MHD perturbations are always in ionization equilibrium.

2.1 The Unperturbed Cloud

We consider here the fluid state representing an unperturbed cloud (denoted by parameters with a 0 subscript) supported by either thermal or magnetic pressure. While the thermally supported cloud is static (but not necessarily stable), ambipolar diffusion in the magnetically supported cloud results in the gradual collapse of the neutral component and the gradual outward diffusion of the ionic and magnetic component (e.g., Shu 1992). However, the requirement that the neutrals are well coupled to the ions (see the discussion before equation [2.5]) implies that the diffusion timescales are longer than the the characteristic MHD timescale. The parameters representing the unperturbed cloud are therefore assumed to be independent of time. With the further constraint that the drift velocity

$$\mathbf{v}_d \equiv \mathbf{v}_{i;0} - \mathbf{v}_0 = \frac{1}{4\pi\gamma C \rho_0^{3/2}} (\nabla \times \mathbf{B}_0) \times \mathbf{B}_0 \tag{2.15}$$

remains smaller than the MHD fluid velocity, the cloud is well approximated by a static state (i.e., $\mathbf{v}_0$=0), and is therefore described by the solutions to

$$4\pi G\rho_0 = -a_s^2 \nabla \cdot \left[\frac{\nabla \rho_0}{\rho_0}\right] + \nabla \cdot \left[\frac{(\nabla \times \mathbf{B}_0) \times \mathbf{B}_0}{4\pi\rho_0}\right] , \tag{2.16}$$

along with a specified relation between the magnetic field and the density.

2.2 The MHD Wave Equation

Linear waves (denoted by parameters with a 1 subscript) propagating through the time-independent unperturbed cloud can be described by a superposition of temporally harmonic perturbations. We therefore consider solutions of the form

$$\rho(\mathbf{x}, t) = \rho_0(\mathbf{x}) + \rho_1(\mathbf{x}) \exp(-i\omega t) , \tag{2.17}$$

where $\Re\{\rho_1\} \ll \rho_0$, and where ρ_0 is a real and known function. With similar assumptions for the remaining parameters $\mathbf{v}$, $\mathbf{B}$, and Φ, the system equations are easily linearized to first order, and the results are given in Appendix A. Since we require $|\mathbf{v}_0| \sim |\mathbf{v}_d| \lesssim |\mathbf{v}_1|$, all $\mathbf{v}_0$ terms are ignored. For a given wave frequency ω, the solutions to these equations describe the spatial structure of the corresponding wave.

As discussed in §2.1, the frequency ω is constrained to be smaller than the neutral collision frequency $\gamma\rho_i$ by the strong coupling condition. Requiring that the lengthscale of the wave is smaller than the lengthscale of the cloud (denoted by R) introduces a lower limit constraint. We therefore consider wave frequencies in the range $\gamma\rho_i \gtrsim \omega \gtrsim 2\pi v_\alpha/R$, where v_α is the Alfvén velocity. Since we are interested in a scenario where waves are continously generated at an assumed location, the frequency is taken to be real. The effects of damping are therefore described by spatial decay in the wave amplitude.

2.3 The Wave-Background Equation

In order to study how the background fluid is affected by the propagation of the MHD waves (with frequency ω), we consider here second order terms. Since these terms (denoted by a 2 subscript) result from the coupling of the real parts of first order terms, their temporal dependence is not purely harmonic, but also includes a time-independent component. We therefore consider solutions of the form

$$\rho(\mathbf{x}, t) = \rho_0(\mathbf{x}) + \Re\{\rho_1(\mathbf{x}) \exp(-i\omega t)\} + \rho_2(\mathbf{x}, t) \tag{2.18}$$

where $\rho_2(\mathbf{x}, t)$ and $\rho_0(\mathbf{x})$ are assumed real, ρ_0 and ρ_1 are known functions, and where $\rho_2 \sim \Re\{\rho_1\}^2$. With a similar assumption made for the remaining variables $\mathbf{v}$, $\mathbf{B}$, and Φ, the system equations are easily linearized to second order (see Appendix B).

Since ω is real, the harmonic parts of the second order terms average to zero over an Alfvén time. This result implies that it is the time independent components which describe the overall effect that the wave has on the background fluid. As such, we time average the second order equations (denoted by $\langle\ \rangle$) with no loss of desired information.

We assume that the continuous propagation of waves through the medium maintains a static time-averaged state, so that

$$\langle \frac{\partial \rho_2}{\partial t} \rangle = \langle \frac{\partial \mathbf{v}_2}{\partial t} \rangle = \langle \frac{\partial \mathbf{B}_2}{\partial t} \rangle = 0 \, . \tag{2.19}$$

Furthermore, since to this order it is no longer valid to ignore $\mathbf{v}_0$ terms, we consider only a perfectly coupled fluid, i.e., we ignore all γ terms and set $\mathbf{v}_0 = 0$. The time-averaged second order equations are presented in Appendix B.

3. 1-D GRADIENT MAGNETOACOUSTIC WAVES

In this section, we study magnetoacoustic waves in the linear limit. Finding general solutions to the linearized equations poses a rather formidable mathematical problem. In order to simplify this task, we consider a slab geometry for the unperturbed state, with only spatial dependence in the $\hat{x}$ direction, and with $\mathbf{B}_0 \equiv B_0 \hat{z}$. The Alfvén speed is taken to be constant throughout the slab, thereby adding the constraint $B_0 \propto \rho_0^{1/2}$. Although these simplifications clearly limit the applicability of the results, they allow an analytical treatment of the problem.

3.1 The Static Solution

In the present geometry, the solutions to equation (2.16) representing the unperturbed static cloud are found to be

$$\rho_0 = \frac{(2a_s^2 + v_\alpha^2)}{4\pi G R^2} \operatorname{sech}^2(\xi) \, , \tag{3.1}$$

and

$$\mathbf{B}_0 = v_\alpha \left(\frac{2a_s^2 + v_\alpha^2}{G R^2} \right)^{1/2} \operatorname{sech}(\xi) \, \hat{z} \, , \tag{3.2}$$

where $\xi = x/R$, and R is the characteristic cloud lengthscale and is related to the column density σ_∞ by

$$R = \frac{2a_s^2 + v_\alpha^2}{2\pi G \sigma_\infty} \, . \tag{3.3}$$

As pointed out by Shu (1983), these solutions correspond to a state which is unstable to Rayleigh-Taylor instabilities on dynamical timescales, although he notes that the instability can be suppressed in a three-dimensional cloud if the lengthscale along the field is shorter than that of the instability. Given these caveats, we treat this case as a model from which to infer information about more realistic (and complex) geometries.

The consequences of this oversimplified geometry are further evidenced in that the effects of ambipolar diffusion become more pronounced away from the central condensation, in direct conflict with observations (Shu 1992). This result is easily seen by noting that the neutral-ion coupling time $(\gamma \rho_i)^{-1} \to \infty$ as $\xi \to \infty$. This divergence is also reflected in the drift velocity, which in the applicable limit that $v_\alpha \gg a_s$, is well approximated by

$$\mathbf{v}_d \approx \frac{v_\alpha}{11.5} \sinh(\xi) \, \hat{x} \, . \tag{3.4}$$

We consider the consequences of this effect below. For now, we note that since $\mathbf{v}_0 \sim \mathbf{v}_d/2$, the omission of the $\nabla \cdot [(\mathbf{v}_0 \cdot \nabla)\mathbf{v}_0]$ term in equation (2.16) is justified only as long as $|\xi| \lesssim 2$, thereby constraining the range over which $\rho_0(\xi)$ and $\mathbf{B}_0(\xi)$ are valid.

3.2 The Wave Solution

The present geometry lends itself to the treatment of magnetoacoustic waves, and we consider the class of solutions where $\mathbf{v}_1 = v_{1x}\hat{x}$ and $\mathbf{B}_1 = B_{1z}\hat{z}$. Indeed, this class of solutions is allowed, and described by the equations of motion (see Appendix A)

$$v_{1x} + A_0 = -\frac{a_s^2 + v_\alpha^2}{\omega^2 R^2}\frac{\partial^2 v_{1x}}{\partial \xi^2} + 2\frac{a_s^2 + v_\alpha^2}{\omega^2 R^2}\tanh(\xi)\,\frac{\partial v_{1x}}{\partial \xi} +$$
$$\frac{1}{\tilde{\gamma}}\,\frac{v_\alpha^4}{(\omega R)^3}\cosh(\xi)\,\frac{\partial}{\partial \xi}\left[\mathrm{sech}(\xi)\frac{\partial}{\partial \xi}\left\{\frac{\partial}{\partial \xi}\frac{B_{1z}}{B_0} - 3\tanh(\xi)\,\frac{B_{1z}}{B_0} + \frac{3}{2}\tanh(\xi)\frac{\rho_1}{\rho_0}\right\}\right], \quad (3.5)$$

$$\frac{B_{1z}}{B_0} = -\frac{i}{\omega R}\frac{\partial v_{1x}}{\partial \xi} + \frac{i}{\omega R}\tanh(\xi)\,v_{1x} +$$
$$\frac{i}{\tilde{\gamma}}\left(\frac{v_\alpha}{\omega R}\right)^2\frac{\partial}{\partial \xi}\left\{\frac{\partial}{\partial \xi}\frac{B_{1z}}{B_0} - 3\tanh(\xi)\,\frac{B_{1z}}{B_0} + \frac{3}{2}\tanh(\xi)\frac{\rho_1}{\rho_0}\right\}, \quad (3.6)$$

and

$$\frac{\rho_1}{\rho_0} = -\frac{i}{\omega R}\frac{\partial v_{1x}}{\partial \xi} + \frac{2\,i}{\omega R}\tanh(\xi)\,v_{1x}\,, \quad (3.7)$$

where A_0 is a constant in x and $\tilde{\gamma} \equiv \gamma R C \rho_0^{1/2}/\omega R$. Notice that equation (3.5) is coupled to equations (3.6) and (3.7) via $\tilde{\gamma}$. Since this parameter represents the ratio of the Alfvén frequency to the neutral coupling frequency, its value must be greater than unity if bulk MHD motion is to be maintained (see the discussion before equation [2.5]). This result suggests that the first order equations may be solved iteratively. However, since $\tilde{\gamma}$ decreases with increasing ξ, the range of validity for an iterative scheme is constrained.

To zeroth order in $\tilde{\gamma}^{-1}$, equation (3.5) may be solved exactly, and the two linearly independent solutions for the velocity are given by

$$v_{1x}\pm = v_{10}\left[\frac{1}{kR}\sinh(\xi) \mp i\cosh(\xi)\right]\exp(\pm ikR\xi) + A_0\,, \quad (3.8)$$

where the constant A_0 must be determined by invoking boundary conditions, and where the wavenumber k is related to ω and R through the dispersion relation

$$\omega^2 = \frac{a_s^2 + v_\alpha^2}{R^2}\left(1 + k^2R^2\right)\,. \quad (3.9)$$

Iterating once to get leading order corrections, and requiring that the full physical solution (including temporal dependence) is real and represent propagation in the positive

ξ direction, we find a solution of the form

$$v_{1x} = v_{10}\left\{\frac{1}{kR}\sinh(\xi)\cos(kR\xi-\omega t+\phi) + \cosh(\xi)\sin(kR\xi-\omega t+\phi) + \right.$$
$$\left.\frac{1}{\tilde{\tilde{\gamma}}}\left(\frac{v_\alpha}{\omega R}\right)^4\left[\Gamma_{vR}\cos(kR\xi-\omega t+\phi)+\Gamma_{vI}\sin(kR\xi-\omega t+\phi)\right]\right\}, \tag{3.10}$$

where Γ_{vR} and Γ_{vI} are given in Appendix C, and where ϕ is the wave phase. With v_{1x} known, we find the density and magnetic fields to be

$$\frac{\rho_1}{\rho_0} = \frac{v_{10}}{\omega R}\left\{\left(\frac{1}{kR}+kR\right)\cosh(\xi)\sin(kR\xi-\omega t+\phi) - \right.$$
$$\frac{2}{kR}\sinh(\xi)\tanh(\xi)\sin(kR\xi-\omega t+\phi) + 2\sinh(\xi)\cos(kR\xi-\omega t+\phi) +$$
$$\left.\frac{1}{\tilde{\tilde{\gamma}}}\left(\frac{v_\alpha}{\omega R}\right)^4\left[\Gamma_{\rho R}\cos(kR\xi-\omega t+\phi)+\Gamma_{\rho I}\sin(kR\xi-\omega t+\phi)\right]\right\}, \tag{3.11}$$

and

$$\frac{B_{1z}}{B_0} = \frac{v_{10}}{\omega R}\left\{\left(\frac{1}{kR}+kR\right)\cosh(\xi)\sin(kR\xi-\omega t+\phi) - \right.$$
$$\frac{1}{kR}\sinh(\xi)\tanh(\xi)\sin(kR\xi-\omega t+\phi) + \sinh(\xi)\cos(kR\xi-\omega t+\phi) +$$
$$\left.\frac{1}{\tilde{\tilde{\gamma}}}\left(\frac{v_\alpha}{\omega R}\right)^4\left[\Gamma_{BR}\cos(kR\xi-\omega t+\phi)+\Gamma_{BI}\sin(kR\xi-\omega t+\phi)\right]\right\}, \tag{3.12}$$

where, again, the Γ terms are given in Appendix C. These solultions are valid to leading order in $1/\tilde{\gamma}$.

Applying the condition that the wavelength must be smaller than the cloud scale height (i.e., $kR \gtrsim 2\pi \gg 1$), one finds that $\rho_1/\rho_0 \sim B_{1z}/B_0 \sim v_{1x}/v_\alpha$, analogous to the case of classical planar magnetoacoustic waves. As such, we focus only on the wave density below, which in the present limit may be approximated by

$$\frac{\rho_1}{\rho_0} \approx \frac{v_{10}}{v_\alpha}\left\{\cosh(\xi)\sin(kR\xi-\omega t+\phi) + \frac{2}{kR}\sinh(\xi)\cos(kR\xi-\omega t+\phi) - \right.$$
$$\left.\frac{1}{\tilde{\tilde{\gamma}}}\cosh(\xi)\cos(kR\xi-\omega t+\phi) + \frac{1}{2kR\tilde{\gamma}}\sinh(\xi)\sin(kR\xi-\omega t+\phi)\right\}. \tag{3.13}$$

The wave amplitude (to this same order) is therefore

$$\left|\frac{\rho_1}{\rho_0}\right| \approx \frac{v_{10}}{v_\alpha}\left[\cosh^2(\xi) + \frac{4}{k^2R^2}\sinh^2(\xi) - \frac{3}{kR\tilde{\gamma}}\sinh(\xi)\cosh(\xi)\right]^{1/2}, \tag{3.14}$$

indicating that magnetic diffusion has the expected effect of damping the wave.

For purposes of illustration, we consider a fluid characterized by $a_s = 0.1$ km s^{-1} and $v_\alpha = 1$ km s^{-1}. We take $v_{10} = 0.1 v_\alpha$, consistant with the static fluid assuption made in §2.1. Figure 1 shows the wave density profile to zeroth order in $\tilde{\gamma}^{-1}$ (i.e., a perfectly coupled fluid) for $kR = 3, 6$ and 10, where the boundary condition $\rho_1|_{\xi=0} = 0$ is used to determine the phase ϕ. It is evident that these solutions are valid only as long as ρ_1 is small compared to ρ_0. Notice that waves propagating down the density gradient will eventually become nonlinear and thereby produce shocks.

In order to determine the validity of the iterative scheme, we introduce the parameter $\eta \equiv |\rho_{1;\tilde{\gamma}}|/\rho_{1;0}|$, where $\rho_{1;\tilde{\gamma}}$ is the part of the wave density due to first order $(\tilde{\gamma})^{-1}$ corrections, and $\rho_{1;0}$ is the wave density in the absence of the corrections. Figure 2 shows the value of η as a function of ξ for $kR = 3, 6$, and 10. It is evident from this figure that the iterative terms are never small when $kR \gtrsim 6$. This finding should not be surprising since the constraints imposed on ω limit the validity of our results to $11.5\ \mathrm{sech}(\xi) > kR$. As the perturbation wavelength decreases, so does the region for which the wave is not strongly damped; this statement is consistent with the aforementioned result that ambipolar diffusion becomes more important away from the cloud center. We present the density profile with first order corrections in Figure 3 for the $kR = 3$ case. Comparing with Figure 1, we see that the inclusion of the ion-neutral drift terms results in both the damping of the wave and an increase in the wavelength. These effects are due to the decrease in the effective fluid density and the corresponding increase in the effective Alfvén speed.

3.3 Wave-Background Interactions

In this section, we determine what effect the propagation of magnetoacoustic waves has on the unperturbed background state. From equation (B2) of Appendix B, the force density resulting from the wave propagation has four forcing terms (i.e., terms coupling two first-order parameters). These terms represent, in order of appearence, the waves' change in momentum, a convective force (analogous to a ram pressure force), a self-gravity force, and a magnetic pressure force. Substituting the solutions found in §3.2, the first two terms are found to result in a compressive force (i.e., a force in the gradient direction), while the latter two terms are found to produce an enhancement force (i.e., a force opposite the gradient direction). The sum of these force components yields the full force density

$$\langle \mathbf{f}_2 \rangle = -\frac{1}{2R}\rho_0 v_{10}^2 \frac{1}{k^2R^2}\left\{ \frac{v_\alpha^2}{\omega^2 R^2}\tanh(\xi) + \frac{4a_s^2}{\omega^2 R^2}\tanh(\xi)\mathrm{sech}^2(\xi)\right\}\hat{x}\ , \tag{3.15}$$

where $\langle\ \rangle$ denotes the time-average over one Alfvén time. Notice that the first two terms in equation (B2) are dominant, and the propagation of the magnetoacoustic waves presented in §3.2 always provides an effective force along the gradient direction, regardless of the propagation direction. This result implies that the overall effect of the waves is to compress the unperturbed state. We note that in the appropriate limit $kR \gg 1$, $\mathbf{f}_2$ scales as $(kR)^{-4} \ll 1$. This point is discussed further below.

The time-averaged mechanical momentum density

$$\langle \mathbf{P}_{mech} \rangle \equiv \langle \rho_1 \mathbf{v}_1 \rangle = \frac{1}{2}\rho_0\big|_{\xi=0} v_{10}^2 \, \frac{k}{\omega}\left(1 + \frac{1}{k^2R^2}\right)\hat{x} \, , \tag{3.16}$$

and the electromagnetic momentum density

$$\langle \mathbf{P}_{em} \rangle \equiv \langle \frac{\mathbf{E}_1 \times \mathbf{B}_1}{4\pi c} \rangle = \frac{1}{2}\rho_0\big|_{\xi=0} v_{10}^2 \, \frac{v_\alpha^2}{c^2}\frac{k}{\omega}\left(1 + \frac{1}{k^2R^2}\right)\hat{x} \, , \tag{3.17}$$

of the wave are both constant in ξ, thus the waves do not gain (or lose) momentum from (to) the background when averaged in time. This result is consistent with the assumption that the time-averaged state is static. For completeness, we note that $\langle \mathbf{P}_{mech} \rangle \gg \langle \mathbf{P}_{em} \rangle$.

The density and magnetic field strength of the compressed state are given by the solutions to

$$\begin{aligned} & a_s^2 \frac{\partial^2}{\partial \xi^2}\frac{\langle \rho_2 \rangle}{\rho_0} + v_\alpha^2 \frac{\partial^2}{\partial \xi^2}\frac{\langle B_{2z} \rangle}{B_0} + v_\alpha^2 \tanh(\xi)\frac{\partial}{\partial \xi}\left(\frac{\langle \rho_2 \rangle}{\rho_0} - 2\frac{\langle B_{2z} \rangle}{B_0}\right) + \\ & 2(a_s^2 + v_\alpha^2)\mathrm{sech}^2(\xi)\frac{\langle \rho_2 \rangle}{\rho_0} - 2v_\alpha^2 \mathrm{sech}^2(\xi)\frac{\langle B_{2z} \rangle}{B_0} = \\ & -\frac{v_{10}^2}{2k^2R^2}\left\{\frac{v_\alpha^2}{\omega^2R^2}\mathrm{sech}^2(\xi) + \frac{4a_s^2}{\omega^2R^2}\left[\mathrm{sech}^4(\xi) - 2\tanh^2(\xi)\mathrm{sech}^2(\xi)\right]\right\} , \end{aligned} \tag{3.18}$$

and by the magnetic induction and continuity equations, which can only be satisfied by the solution

$$\langle v_{2x} \rangle = -\frac{v_{10}^2}{2}\frac{kR}{\omega R}\left[1 + \frac{1}{k^2R^2}\right]\cosh^2(\xi) \, . \tag{3.19}$$

In order to get a fully analytical expression, a relation between $\langle \rho_2 \rangle$ and $\langle B_{2z} \rangle$ must be specified. As a simple example, we consider here the limit that $B \to 0$, corresponding to planar sound propagation through a thermally supported slab. Equation (3.18) thus reduces to

$$a_s^2 \frac{\partial^2}{\partial \xi^2}\frac{\langle \rho_2 \rangle}{\rho_0} + 2a_s^2 \mathrm{sech}^2(\xi)\frac{\langle \rho_2 \rangle}{\rho_0} = \frac{v_{10}^2}{2k^2R^2}\frac{4a_s^2}{\omega^2R^2}\left[2\tanh^2(\xi)\mathrm{sech}^2(\xi) - \mathrm{sech}^4(\xi)\right] \, . \tag{3.20}$$

Using the method of variation of parameters, we find the general solution to be

$$\frac{\langle \rho_2 \rangle}{\rho_0} = \frac{2v_{10}^2}{\omega^2k^2R^4}\left[\frac{3}{4}\mathrm{sech}^2(\xi) - \frac{1}{2}\right] + A_1 \tanh(\xi) + A_2\left[\xi\tanh(\xi) - 1\right] , \tag{3.21}$$

where A_1 and A_2 are constants. The form of the effective force (equation [3.15]) implies that $\langle \rho_2 \rangle$ must be an even function. Furthermore, conservation of mass requires that

$$\int_0^\infty \langle \rho_2 \rangle \, d\xi = 0 \, . \tag{3.22}$$

These two constraints imply that the constants A_1 and A_2 must be zero.

The time-averaged density component $\langle \rho_2 \rangle$ is shown in Figure 4 for various physical parameters. As shown by equation (3.21), the resulting time-averaged state corresponds to a compression of the initially unperturbed state. The dependence of the second-order force on the wavelength is reflected in $\langle \rho_2 \rangle$ since $v_{10}^2/\omega^2 R^2 k^2 R^2 \approx v_{10}^2/a_s^2 k^4 R^4 \ll 1$. Since this quantity is small compared to unity, the waves have a minimal effect on the background. The compression is therefore quite small even for large amplitude waves. From the form of the force density, it is evident that this result must also be true for the general case where B is nonzero.

The compression resulting from the wave propagation is unique to the nonhomogeneous fluid in that wave dissipation is not required to provide a momentum transfer to the background. Furthermore, the second-order force on the fluid is not dependent on the propagation direction. It is reasonable to assume that the inclusion of dissipative effects will result in a pressure gradient along the propagation direction.

4. 1-D GRADIENT ALFVÉN WAVES

In this section, we study Alfvén waves in the linear limit. We present an analogous format to §3, but for a slab geometry assumed for the unperturbed state with only a z spatial dependence and with $\mathbf{B}_0 \equiv B_0 \hat{z}$. The divergenceless condition constrains B_0 to be constant. As discussed in §4.3, we find that Alfvén waves can help support clouds against gravitational collapse.

4.1 The Static Solution

We begin with the static configuration. In the present geometry, the solution to equation (2.16) representing the static cloud is found to be

$$\rho_0 = \frac{a_s^2}{2\pi G R^2} \operatorname{sech}^2(\xi) , \tag{4.1}$$

where $\xi \equiv z/R$ and R is a characteristic lengthscale that is related to the column density σ_∞ by

$$R = \frac{a_s^2}{\pi G \sigma_\infty} . \tag{4.2}$$

This density distribution corresponds to a truly static, thermally supported state (i.e., ambipolar diffusion is absent, so that $\mathbf{v}_d = 0$). In contrast to an isothermal sphere, the thermally supported slab is never gravitationally unstable.

4.2 The Wave Solution

In this geometry we study of Alfvén waves, and here we consider the class of solutions where $\mathbf{v}_1 = v_{1x}\hat{x}$ and $\mathbf{B}_1 = B_{1x}\hat{x}$. Indeed, this class of solutions is allowed and results

in uncompressed fluid motion. Hence, the wave density $\rho_1 = 0$, analogous to the classical Alfvén waves, and the velocity is described by the equation

$$\frac{d^2 v_{1x}}{d\xi^2} + \frac{1}{1+\tilde{\gamma}^{-2}}\Big(\frac{2}{\tilde{\gamma}^2}\tanh(\xi)\frac{dv_{1x}}{d\xi} - \frac{2i}{\tilde{\gamma}}\tanh(\xi)\frac{dv_{1x}}{d\xi} + \frac{1}{\tilde{\gamma}^2}v_{1x} - \frac{i}{\tilde{\gamma}}v_{1x} + K^2R^2\mathrm{sech}^2(\xi)v_{1x} + \frac{i}{\tilde{\gamma}}K^2R^2\mathrm{sech}^2(\xi)v_{1x}\Big) = 0\,, \tag{4.3}$$

where $\tilde{\gamma} \equiv \gamma RC\ \rho_0^{1/2}/\omega R$ is the coupling parameter introduced in §3.2, and where we have defined $KR \equiv \omega R\ /v_\alpha\ |_{\xi=0}$. With $\rho_1 = 0$, it is also possible to find the equation describing B_{1x}, i.e.,

$$\frac{d^2 B_{1x}}{d\xi^2} + \frac{1}{1+\tilde{\gamma}^{-2}}\Big[\Big(2 - \frac{i}{\tilde{\gamma}} + \frac{3}{\tilde{\gamma}^2}\Big)\tanh(\xi)\frac{dB_{1x}}{d\xi} + \Big(1+\frac{i}{\tilde{\gamma}}\Big)K^2R^2\mathrm{sech}^2(\xi)B_{1x}\Big] = 0\,. \tag{4.4}$$

Notice that the amplitudes of B_{1x} and v_{1x} are coupled through the magnetic induction equation.

The requirment that the wavelength is smaller than the cloud scale height implies that $KR \gtrsim 2\pi \gg 1$. Furthermore, the requirement that the waves are not quickly damped due to magnetic diffusion constrains $\tilde{\gamma}$ to be larger that unity. We therefore consider a parameter space $(a_s, v_\alpha, \omega; \xi)$ where both of these conditions are satisfied. The relation

$$\tilde{\gamma}KR = 16\ \frac{a_s}{v_\alpha|_{\xi=0}}\ \mathrm{sech}(\xi) \tag{4.5}$$

implies that a limited range of parameters will be consistent with our assumptions. With $KR \gg 1$ and $\tilde{\gamma} \gg 1$, equation (4.3) may be solved by assuming a solution of the form $v_{1x} = v_{1x0}\ \exp(i\phi)$. With $kr \equiv \phi'$, where $'$ denotes differentiation by ξ, one finds (to second order in KR and $\tilde{\gamma}^{-1}$)

$$ikR = iKR\Big(1 + \frac{1}{8K^2R^2}\Big)\mathrm{sech}(\xi) + \frac{i}{8KR}\cosh(\xi) + \frac{1}{2}\tanh(\xi) - \frac{KR}{2\tilde{\gamma}}\mathrm{sech}(\xi) - i\frac{3KR}{8\tilde{\gamma}^2}\mathrm{sech}(\xi) + i\frac{3}{4\tilde{\gamma}}\tanh(\xi)\,. \tag{4.6}$$

Requiring that the full physical solution (including temporal dependence) be real and represent proapgation in the positive ξ direction, one finds

$$v_{1x} = v_{1x0}\cosh(\xi)^{1/2}\exp\Big(-\frac{KR}{2\tilde{\gamma}_0}\xi\Big)\cos\Big[KR\Big(1+\frac{1}{K^2R^2}\Big)\tan^{-1}[\sinh(\xi)] + \frac{1}{8KR}\sinh(\xi) - \frac{3KR}{8\tilde{\gamma}_0^2}\sinh(\xi) + \frac{3}{4\tilde{\gamma}_0}\cosh(\xi) - \omega t + \phi\Big]\,, \tag{4.7}$$

where $\tilde{\gamma}_0$ represents $\tilde{\gamma}$ evaluated at $\xi = 0$, and ϕ is the phase of the wave; this phase must be determined by invoking boundary conditions. An analogous treatment for the magnetic field component yields the full solution

$$B_{1x} = B_{1x0}\ \mathrm{sech}(\xi)^{1/2}\ \exp\Big(\frac{-KR}{2\tilde{\gamma}_0}\xi\Big)\ \cos\Big[KR\Big(1+\frac{1}{K^2R^2}\Big)\tan^{-1}[\sinh(\xi)] - \frac{3}{8KR}\sinh(\xi) - \frac{3KR}{8\tilde{\gamma}_0^2}\sinh(\xi) + \frac{1}{4\tilde{\gamma}_0}\cosh(\xi) - \omega t + \phi\Big]\ . \tag{4.8}$$

Since equations (4.2) and (4.3) can also be solved numerically, the validity of these results are easily checked (see below).

For illustrative purpose, we consider a fluid characterized by $a_s = 0.2$ km s^{-1} and $v_\alpha|_{\xi=2} = 1$ km s^{-1}. Since $v_{1x} \sim B_{1x}\ \cosh(\xi)$, we only present the analytical solution for B_{1x} as a function of ξ (see Figure 5). In this case, the wave phase ϕ is determined by applying the boundary condition $B_{1x}|_{\xi=0,t=0} = 0$. We consider frequencies corresponding to $KR = 6$ ($\tilde{\gamma}_0 = 7.5$) and $KR = 10$ ($\tilde{\gamma}_0 = 4.5$). Numerical solutions are also included. To illustrate the effects of magnetic diffusion, we also consider the same values of KR in the artificial limit $\tilde{\gamma} \to \infty$. These results are presented in Figure 6. Notice that magnetic diffusion plays a crucial role in the propagation of the waves, and that only a very narrow band of parameter space consistent with cloud environments allows wave propagation without strong attenuation.

4.3 Wave-Background Interactions

In this section, we determine what effect the propagation of Alfvén waves has on the unperturbed background state. From Appendix B and equation (4.8), we find that the second-order time-averaged force due to the wave action results only from a magnetic pressure gradient, and may be expressed as

$$\langle \mathbf{f}_2 \rangle = \frac{1}{16\pi R}\ B_{1x0}^2\ \mathrm{sech}(\xi)\tanh(\xi)\ \hat{z}\ . \tag{4.9}$$

As in the case of magnetoacoustic waves (§3), this force is independent of the propagation direction. However, the effect of this force on the background fluid is to enhance the density away from the cloud center. Notice that the average force given by equation (4.9) is positive (for $\xi > 0$), whereas that due to the magnetoacoustic waves (equation [3.15]) has the oppposite sign. Since the time-averaged wave pressure, which is purely electromagnetic, is a constant in ξ, i.e.,

$$\langle \mathbf{P} \rangle \equiv \langle \frac{\mathbf{E}_1 \times \mathbf{B}_1}{4\pi c} \rangle = \frac{-B_{1x0}\ v_{1x0}\ B_0}{4\pi c^2}\ \hat{z} + \text{higher order terms}\ , \tag{4.10}$$

the waves do not gain (or lose) momentum from (to) the background when averaged in time. This result is consistent with the assumption that the second order time-averaged state is static.

The second order perturbation density $\langle\rho_2\rangle$ is described by the equation

$$\frac{d^2}{d\xi^2}\frac{\langle\rho_2\rangle}{\rho_0} + 2\mathrm{sech}^2(\xi)\frac{\langle\rho_2\rangle}{\rho_0} = \left(\frac{B_{1x0}}{B_0}\right)^2 \frac{v_\alpha^2|_{\xi=0}}{4a_s^2}\cosh(\xi) \ . \tag{4.11}$$

Using the method of variation of parameters, the general solution is found to be

$$\frac{\langle\rho_2\rangle}{\rho_0} = \left(\frac{B_{1x0}}{B_0}\right)^2 \frac{v_\alpha^2|_{\xi=0}}{4a_s^2}\left[\cosh(\xi) - 2\mathrm{sech}^2(\xi)\right] + A_1\tanh(\xi) + A_2[\xi\tanh(\xi) - 1] \ . \tag{4.12}$$

Since the force responsible for this density perturbation is symmetric about the origin, $\langle\rho_2\rangle$ must be an even function. Furthermore, mass conservation requires that

$$\int_0^\infty \langle\rho_2\rangle d\xi = 0 \ . \tag{4.13}$$

These constraints imply that the constants A_1 and A_2 must be zero.

The total time averaged density as a function of ξ is shown in Figure 7 for various parameters. Notice that this function is independent of wavelength. Notice also that larger amplitude waves are capable of displacing and supporting a larger mass away from the equilibrium state. This result suggests that Alfvén waves are capable of helping to support clouds against gravitational collapse along field lines. It should be pointed out, however, that our results are valid only as long as $\rho_2 \ll \rho_0$. Notice also that the presence of ion-neutral drift results in appreciable wave damping and subsequent momentum transfer to the background medium. Our results should therefore be taken as a lower limit to the overall density enhancement.

5. APPLICATION TO OBSERVATIONS

In this section, we consider our results in the context of the clumps observed in giant molecular cloud complexes. These structures are characterized by size scales $L \sim 2-5$ pc and column densities $\sigma_\infty \sim 0.01$ g cm^{-2}, thereby implying central densities on the order of $n \sim 500$ cm^{-3}. Furthermore, typical temperatures and field strengths are found to be $T \sim 10$ K and $B \sim 30\mu$G, respectively (for a discussion on the physical properties of cloud environments, see e.g. Mouschovias 1987; Heiles 1987; Falgorne & Puget 1988; Blitz 1992; and references therein).

5.1 The Magnetoacoustic Waves

The geometry presented in §3, where we study magnetoacoustic waves, corresponds to a state of maximal magnetic support. Equations (3.1) and (3.2) therefore imply a relation between the magnetic field and the total supported column density $B_0 = 4\pi G^{1/2}\sigma_\infty$. By considering a slab with extension in y and z of length $2R$, one finds that the mass supported by the enclosed magnetic flux is equal to the magnetic Jean's mass (Shu et. al 1987) .

For typical clump column densities, the magnetic field strength at the slab center (in our model) is $B \approx 30\mu$G, in rough agreement with observations. Furthermore, the scale-height R is not constrained to any specific value, and may be chosen to fit any observational

data. This finding confirms the well known result that a static magnetic pressure is capable of providing cloud support across the field lines. As such, the finding that magnetohydrodynamic waves may in fact compress the initially static fluid is not in contradiction with observations. Indeed, since the magnitude of the compression force scales as $(kR)^{-4}$, the resulting effects must be negligible for the wave modes considered here.

The propagation of MHD waves through a medium results in velocity fluctuations of the entire fluid. Assuming that the observed molecular lines have a characteristic width Δv which scales as the amplitude of the fluid velocity (i.e., $\Delta v \sim |\mathbf{v}_1|$), we find that our results reproduce the observed parametric relation $\Delta v \sim \rho_0^{-1/2}$. Since the Alfvén speed scales similarly (i.e., $v_\alpha \propto \rho^{-1/2}$), it has been suggested that Δv also scales as v_α (e.g., Elmegreen 1990). For the present case, however, the Alfvén speed is constant throughout the cloud region, but the velocity amplitudes of our waves do increase with distance from the cloud center. In the limit that magnetic diffusion is ignored, we find

$$\Delta v = v_{10} \left[(1 + \frac{1}{k^2 R^2}) \cosh^2(\xi) - \frac{1}{k^2 R^2} \right]^{1/2} . \tag{5.1}$$

This result is consistent with the general observational feature that line-widths increase away from the cloud center, although the observed spatial relationship $\Delta v \sim \xi^{1/2}$ is not found here (see, e.g., Myers & Fuller 1992). However, this discrepency is not surprising due to the limitations of our geometry.

Several dissipative mechanisms exist in molecular clouds that may play a significant role in the propagation of MHD waves. Although we do not consider the important nonlinear processes of wave steepening and mode-mode coupling (Zweibel & Josafatsson 1983), we do include the dissipative effects of magnetic diffusion. Notice that for these former effects the resulting damping lengthscale for waves produced at the origin is comparable to the wavelength. We note, however, that the density in physical clouds is observed to scale as $\rho \sim \xi^{-1}$, corresponding to an ion density that scales as $\rho_i \sim \xi^{-1/2}$. In contrast, the density of the magnetically supported slab is proportional to $\mathrm{sech}(\xi) \sim \exp(-\xi)$, and as a result, the dissipative effects in our model become much more pronounced with distance than in actual clouds. Indeed, consider that in real clouds, the neutral coupling scales as $(\rho_i \gamma)^{-1} \sim \xi^{1/2}$, whereas the characteristic Alfvén time scales as $\omega^{-1} \sim k^{-1} \sim \xi$. This finding implies that the damping effects in these environments become less important as the scaleheight increases. This behavior is opposite to what is found in the slab geometry, where the neutral coupling time $(\rho_i \gamma)^{-1} \sim \exp(\xi)$. Thus, it is clear that the ion-neutral dissipative effects have an artificial ξ dependence resulting from the assumed geometry, and the limiting case $\gamma \rightarrow \infty$ may be more representative of actual physical situations. Alternatively, a cloud with an initial slab-like density profile may be strongly modified by the resulting wave pressure, and ultimately end up with a enhanced density profile more favorable to wave propagation. A proper treatment of such an effect is beyond the scope of simple linear theory, and should be the subject of future work.

5.2 The Alfvén Waves

We now consider the case of Alfvén waves. For the thermally supported slab presented in §4, equations (4.1) and (4.2) indicate that the observed column densities correspond to a cloud scale-height $R \sim 0.02$ pc (along the field line direction), in sharp contrast to the typical cloud scalelengths of $\sim 2 - 5$ pc. Thus, nonthermal processes must be present and must provide a supporting pressure along the field line direction; the results of §4.3 indicate that outwardly propagating Alfvén waves are a viable candidate. Although the effects of wave damping due to ion-neutral slipping have been ignored, it is reasonable to assume that their inclusion only adds to the cloud support by providing a steeper pressure gradient. We emphasize, however, that our results are limited in that their validity breaks down when $\langle \rho_2 \rangle$ is comparable to ρ_0. As a result, this simple linear theory is inadequate to calculate any appreciable cloud support. In light of this complication, a more complete semi-linear treatment of the problem is currently being considered.

As discussed in §5.1, the propagation of MHD waves through a medium results in velocity fluctuations of the entire fluid. Using the same assumption for the relation between the characteristic widths of the observed molecular lines and the fluid velocity, we find that

$$\Delta v = v_{10} \cosh^{1/2}(\xi) \ , \tag{5.2}$$

where we have taken the limit that magnetic diffusion is negligible. Although the general observational feature that line widths increase with "radius" is exhibited by our solutions, they do not fit the observed spatial relation $\Delta v \sim \xi^{1/2}$. Notice that the Alfvén speed v_α has an even stronger dependence on ξ than does v_{1x}. In contrast to the magnetoacoustic waves, these Alfvén waves satisfy a parametric relation $\Delta v \sim \rho_0^{-1/4}$. These results could partially be an artifact of the initial density profile, which is not characteristic of the observed clouds, and is expected to be strongly modified by the presence of these waves. It is interesting that the wave amplitude may be described by the relation $\Delta v \sim \langle \rho_2 \rangle^{-1/2}$, in analogy to the observations.

As with the magnetoacoustic waves, the effects of magnetic diffusion play an important role in Alfvén wave propagation. For reasonable cloud parameters, these waves are found to damp on lengthscales shorter than wavelength. A discussion of the interpretation of these results is similar to that given for the magnetoacoustic waves in §5.1.

6. SUMMARY AND CONCLUSIONS

In this paper, we have studied how MHD waves propagate through nonhomogeneous, self-gravitating media representative of molecular cloud environments. In order to obtain analytic results, we have considered two simplifying slab geometries. In particular, we have considered magnetoacoustic wave propagation in a magnetically supported slab, and Alfvén wave propagation in a thermally supported slab. Although these simplifying geometries are somewhat artificial compared to actual physical clouds, some general conclusions can be made:

(1) The MHD wave component of the fluid velocity increases with decreasing density. Assuming that this velocity characterizes the molecular line widths, we find that this

result is in rough agreement with observations, although we do not reproduce the spatial relationship $\Delta v \propto \xi^{1/2}$. We stress, however, that magnetoacoustic wave propagation in this geometry does reproduce the observed relation between density and linewidth $\Delta v \sim \rho^{-1/2}$. For the Alfvén wave propagation, we obtain the relationship $\Delta v \sim \rho_0^{-1/4}$, which is in qualitative but *not* in quantitative agreement with observations.

(2) Alfvén waves are capable of providing support along the field line direction, even in the absence of damping. The wave motion results in a second order time averaged back-reaction force which is exerted on the background fluid. For Alfvén waves, this time-averaged force is capable of providing considerable density support. For the magnetoacoustic wave scenario, this force compresses the unperturbed state, although the overall effect is minimal since the magnitude of the force scales as $(kR)^{-4}$. We stress that the back-reaction force does not result from wave-damping and is independent of the propagation direction.

(3) Magnetic diffusion may play an important role in cloud dynamics and can result in strong wave dissipation and subsequent momentum transfer to the fluid. However, the results found for our simplified geometries are in conflict with observations in that the effects of magnetic diffusion become more pronounced away from the cloud center. In addition, we note that competing nonlinear dissipative mechanisms (i.e., wave steepening and mode-mode coupling) have been ignored, and should be included in future work.

The idea that observed line-widths in molecular clouds is due to MHD wave motion has been discussed previously (Arons & Max 1975; Zweibel & Josafatsson 1983). This paper is an extension of previous work in that we calculate how velocity perturbations behave in nonuniform media. However, a complete treatment which simultaneously considers dissipation, nonlinearity, and nonuniformity is still needed.

Acknowledgements

We would like to thank Bruce Elmegreen and Phil Myers for useful discussions. This work was supported by NASA Grant Nos. NAGW–2802 and NAGW-3121, and by funds from the Physics Department at the University of Michigan.

APPENDIX A: FIRST ORDER EQUATIONS

In this Appendix, we write down the linearized forms of equations (2.6) – (2.10) to first order. In the applicable limit that $|\mathbf{v}_d| \lesssim |\mathbf{v}_1|$, the $\mathbf{v}_0$ terms are justifiably ignored. Substituting solutions of the form given by equation (2.17), we find that the first order equations reduce to

$$-i\omega\mathbf{v}_1 = -\nabla\Phi_1 - a_s^2\nabla\left(\frac{\rho_1}{\rho_0}\right) + \frac{(\nabla\times\mathbf{B}_1)\times\mathbf{B}_0}{4\pi\rho_0} + \frac{(\nabla\times\mathbf{B}_0)\times\mathbf{B}_1}{4\pi\rho_0} - \frac{\rho_1}{\rho_0}\frac{(\nabla\times\mathbf{B}_0)\times\mathbf{B}_0}{4\pi\rho_0}, \tag{A1}$$

$$-i\omega \mathbf{B}_1 = \nabla \times (\mathbf{v}_1 \times \mathbf{B}_0) + \mathbf{D}_1 \ , \tag{A2}$$

where

$$\mathbf{D}_1 = \nabla \times \left[\frac{1}{4\pi\gamma C \rho_0^{3/2}} \left\{ [(\nabla \times \mathbf{B}_1) \times \mathbf{B}_0] \times \mathbf{B}_0 + [(\nabla \times \mathbf{B}_0) \times \mathbf{B}_1] \times \mathbf{B}_0 + \right.\right.$$
$$\left.\left. [(\nabla \times \mathbf{B}_0) \times \mathbf{B}_0] \times \mathbf{B}_1 - \left(\frac{3\rho_1}{2\rho_0}\right) [(\nabla \times \mathbf{B}_0) \times \mathbf{B}_0] \times \mathbf{B}_0 \right\} \right] , \tag{A3}$$

$$-i\omega \rho_1 + \nabla \cdot (\mathbf{v}_1 \ \rho_0) = 0 \ , \tag{A4}$$

and

$$\nabla^2 \Phi_1 = 4\pi G \rho_1 \ . \tag{A5}$$

These equations may be combined to yield

$$\omega^2 \nabla \cdot \mathbf{v}_1 = -a_s^2 \nabla^2 \left[\frac{\nabla \cdot (\rho_0 \mathbf{v}_1)}{\rho_0} \right] - 4\pi G \nabla \cdot (\rho_0 \mathbf{v}_1) -$$
$$\nabla \cdot \left[\frac{(\nabla \times \{\nabla \times [\mathbf{v}_1 \times \mathbf{B}_0]\}) \times \mathbf{B}_0}{4\pi\rho_0} + \frac{(\nabla \times \mathbf{B}_0) \times \{\nabla \times [\mathbf{v}_1 \times \mathbf{B}_0]\})}{4\pi\rho_0} \right] -$$
$$\nabla \cdot \left[\frac{\nabla \cdot (\rho_0 \mathbf{v}_1)}{\rho_0} \ \frac{(\nabla \times \mathbf{B}_0) \times \mathbf{B}_0}{4\pi\rho_0} \right] - \nabla \cdot \left[\frac{(\nabla \times \mathbf{D}_1) \times \mathbf{B}_0}{4\pi\rho_0} + \frac{(\nabla \times \mathbf{B}_0) \times \mathbf{D}_1}{4\pi\rho_0} \right] , \tag{A6}$$

and

$$\omega^2 \nabla \times \mathbf{v}_1 = -\nabla \times \left[\frac{(\nabla \times \{\nabla \times [\mathbf{v}_1 \times \mathbf{B}_0]\}) \times \mathbf{B}_0}{4\pi\rho_0} + \frac{(\nabla \times \mathbf{B}_0) \times \{\nabla \times [\mathbf{v}_1 \times \mathbf{B}_0]\})}{4\pi\rho_0} \right] -$$
$$\nabla \times \left[\frac{\nabla \cdot (\rho_0 \mathbf{v}_1)}{\rho_0} \ \frac{(\nabla \times \mathbf{B}_0) \times \mathbf{B}_0}{4\pi\rho_0} \right] - \nabla \times \left[\frac{(\nabla \times \mathbf{D}_1) \times \mathbf{B}_0}{4\pi\rho_0} + \frac{(\nabla \times \mathbf{B}_0) \times \mathbf{D}_1}{4\pi\rho_0} \right] . \tag{A7}$$

Notice that in the fully coupled fluid limit (i.e., $\gamma \to \infty$) equations (A6) and (A7) decouple from the other first order equations.

APPENDIX B: SECOND ORDER EQUATIONS

In this Appendix, we write down the linearized forms of equations (2.6) – (2.10) to second order. For simplicity, we assume that the ions and neutrals are perfectly coupled, so that $\mathbf{v}_0 = 0$, and the γ terms are ignored. Substituting solutions of the form given by equation (2.18) and time-averaging over one Alfvén time, the second order equations reduce to

$$a_s^2 \langle \nabla \rho_2 \rangle + \rho_0 \langle \nabla \Phi_2 \rangle + \langle \rho_2 \rangle \nabla \Phi_0 - \frac{(\nabla \times \langle \mathbf{B}_2 \rangle) \times \mathbf{B}_0}{4\pi} - \frac{(\nabla \times \mathbf{B}_0) \times \langle \mathbf{B}_2 \rangle}{4\pi} = \langle \mathbf{f}_2 \rangle \ , \tag{B1}$$

where

$$\mathbf{f}_2 = -\rho_1 \frac{\partial \mathbf{v}_1}{\partial t} - \rho_0 \mathbf{v}_1 \cdot \nabla \mathbf{v}_1 - \rho_1 \nabla \Phi_1 + \frac{(\nabla \times \mathbf{B}_1) \times \mathbf{B}_1}{4\pi} \ , \tag{B2}$$

$$\nabla \times (\langle \mathbf{v}_1 \times \mathbf{B}_1 \rangle + \langle \mathbf{v}_2 \rangle \times \mathbf{B}_0) = 0 \ , \tag{B3}$$

$$\nabla \cdot (\langle \mathbf{v}_1 \rho_1 \rangle + \langle \mathbf{v}_2 \rangle \rho_0) = 0 \ , \tag{B4}$$

and

$$\nabla^2 \langle \Phi_2 \rangle = 4\pi G \langle \rho_2 \rangle \ , \tag{B5}$$

where $\langle \ \rangle$ symbolizes the time-averaging operation, and the time-average of a time derivative is assumed equal to zero (see §2.2).

These equations may be combined to yield

$$\begin{aligned} & a_s^2 \nabla^2 \left[\frac{\langle \rho_2 \rangle}{\rho_0} \right] + 4\pi G \langle \rho_2 \rangle + \nabla \cdot \left[\frac{\langle \rho_2 \rangle}{\rho_0} \frac{(\nabla \times \mathbf{B}_0) \times \mathbf{B}_0}{4\pi \rho_0} \right] - \\ & \nabla \cdot \left[\frac{(\nabla \times \langle \mathbf{B}_2 \rangle) \times \mathbf{B}_0}{4\pi \rho_0} + \frac{(\nabla \times \mathbf{B}_0) \times \langle \mathbf{B}_2 \rangle)}{4\pi \rho_0} \right] = \\ & \langle -\nabla \cdot (\mathbf{v}_1 \cdot \nabla \mathbf{v}_1) + \frac{a_s^2}{2} \nabla^2 \left(\frac{\rho_1}{\rho_0} \right)^2 + \nabla \cdot \left[\frac{(\nabla \times \mathbf{B}_1) \times \mathbf{B}_1}{4\pi \rho_0} \right] + \\ & \nabla \cdot \left[\frac{\rho_1^2}{\rho_0^2} \frac{(\nabla \times \mathbf{B}_0) \times \mathbf{B}_0}{4\pi \rho_0} - \frac{\rho_1}{\rho_0} \frac{(\nabla \times \mathbf{B}_1) \times \mathbf{B}_0}{4\pi \rho_0} - \frac{\rho_1}{\rho_0} \frac{(\nabla \times \mathbf{B}_0) \times \mathbf{B}_1}{4\pi \rho_0} \right] \rangle \ . \end{aligned} \tag{B6}$$

In obtaining equation (B6), we have used the zeroeth and first order equations of motion to eliminate the gravitational potentials Φ_0 and Φ_1, respectively.

APPENDIX C: THE Γ PARAMETERS

In this Appendix we define the Γ parameters introduced in §3.2. These are:

$$\Gamma_{vR} \equiv -\frac{1}{2}(1 + k^2R^2)(3 + 2k^2R^2)\cosh(\xi) + \frac{3}{2}(3 - k^2R^2)\mathrm{sech}(\xi) - 8\mathrm{sech}^3(\xi) \ , \tag{C1}$$

$$\Gamma_{vI} \equiv \frac{\sinh(\xi)}{2kR} \left[(1 + k^2R^2)k^2R^2 + 4(-1 + 2k^2R^2)\mathrm{sech}^2(\xi) + 16\mathrm{sech}^4(\xi) \right] \ , \tag{C2}$$

$$\begin{aligned} \Gamma_{\rho R} = & -\frac{1}{kR} \Big[\frac{1}{2}(1 + k^2R^2)(3 + 2k^2R^2)k^2R^2\cosh(\xi) + \\ & (4 - 12k^2R^2 + 2k^4R^4)\mathrm{sech}(\xi) + (-38 + 20k^2R^2)\mathrm{sech}^3(\xi) + 40\mathrm{sech}^5(\xi) \Big] \ , \end{aligned} \tag{C3}$$

$$\Gamma_{\rho I} = \frac{\sinh(\xi)}{2} \left[(1 + k^2R^2)k^2R^2 + (-22 + 14k^2R^2)\mathrm{sech}^2(\xi) + 80\mathrm{sech}^4(\xi) \right] \ , \tag{C4}$$

$$\Gamma_{BR} = \frac{-1}{kR}\Bigg[(1+k^2R^2)(2+k^2R^2)k^2R^2\cosh(\xi)+$$

$$\frac{1}{2}(4-17k^2R^2+3k^4R^4)\mathrm{sech}(\xi)+(-28+16k^2R^2)\mathrm{sech}^3(\xi)+32\mathrm{sech}^5(\xi)\Bigg]+$$

$$\frac{\omega^2R^2}{kRv_\alpha^2}\left[\frac{1}{2}(-3-5k^2R^2-2k^4R^4)\cosh(\xi)+(1-k^2R^2)\mathrm{sech}(\xi)-2\mathrm{sech}^3(\xi)\right], \quad \text{(C5)}$$

and

$$\Gamma_{BI} = \sinh(\xi)\Bigg[\frac{1}{2}(1+k^2R^2)(-3-k^2R^2)+\frac{1}{2}(-13+11k^2R^2)\mathrm{sech}^2(\xi)+$$

$$32\mathrm{sech}^4(\xi)\Bigg]+\frac{\omega^2R^2}{v_\alpha^2}\sinh(\xi)\left[\frac{1}{2}(1+k^2R^2)+2\mathrm{sech}^2(\xi)\right]. \quad \text{(C6)}$$

REFERENCES

Arons, J., & Max, C. E. 1975, *ApJ*, **196**, L77

Blitz, L. 1992, in Protostars and Planets III, ed. E. Levy and M. S. Mathews (Tucson: University of Arizona Press), in press

Bonazzola, S., et. al. 1987, *A & A*, **172**, 293

Chandrasekhar, S., & Fermi, E. 1953, *ApJ*, **118**, 116

Dewar, R. L. 1970, *Phys. Fluids*, **13**, 2710

Draine, B. T., Roberge, W., & Dalgarno, A. 1983, *ApJ*, **270**, 519

Elmegreen, B. G. 1979, *ApJ*, **232**, 729

Elmegreen, B. G. 1985, *ApJ*, **299**, 196

Elmegreen, B. G. 1990, *ApJ*, **361**, L77

Falgorne, E., & Puget, J. L. 1986, *A & A*, **162**, 235

Falgorne, E., & Puget, J. L. 1988, in Galactic and Extragalactic Star Formation, ed. R. E. Pudritz and M. Fich (Dordrecht: Kluwer Academic Publishers), p. 195

Goodman, A. A., Crutcher R. M., Heiles, C., Myers, P. C., & Troland, T. H. 1989, *ApJ*, **338**, 161

Goodman, A. A. 1990, PhD Thesis, Harvard University

Heiles, C. 1987, in Physical Processes in Interstellar Clouds, ed. G. E. Morfill and M. Scholer (Dordrecht: Reidel), p. 429

Houlahan, P., & Scalo, J. 1992, *ApJ*, **393**, 172

Kazés, I., et al. 1987, in Galactic and Extragalactic Star Formation, ed. R. E. Pudritz and M. Fich (Dordrecht: Reidel), p. 291

Larson, R. B. 1981, *MNRAS*, **194**, 809

Mestel, L. 1965, *QJRAS*, **6**, 161

Mouschovias, T. Ch. 1976, *ApJ*, **207**, 141

Mouschovias, T. Ch. 1987, in Physical Processes in Interstellar Clouds, ed. G. E. Morfill and M. Scholer (Dordrecht: Reidel), p. 453

Mouschovias, T. Ch., & Spitzer, L. 1976, *ApJ*, **210**, 326

Murphy, D. C., & Myers, P. C. 1985, *ApJ*, **298**, 818

Myers, P. C., & Goodman, A. 1988, *ApJ*, **326**, L27

Myers, P. C., & Fuller, G. A. 1992, *ApJ*, **396**, 631

Nishi, R., Nakano, T., & Umebayashi, T. 1991, *ApJ*, **368**, 181

Oppenheimer, M., & Dalgarno, A. 1974, *ApJ*, **192**, 29

Pudritz, R. E. 1990, *ApJ*, **350**, 195

Schwarz, U. J., et. al. 1986, *ApJ*, **301**, 320

Shu, F. H. 1983, *ApJ*, **273**, 202

Shu, F. H. 1992, Gas Dynamics (Mill Valley: University Science Books)

Shu, F. H., Adams, F. C., & Lizano, S. 1987, *ARA&A*, **25**, 23

Spitzer, L. 1968, Nebulae and Interstellar Matter; Stars and Stellar Systems, ed. B. Middlehurst and L. H. Aller (Chicago: University Press) 7:1

Strittmatter, P. A. 1966, *MNRAS*, **132**, 359

Wiseman, J. J., & Adams, F. C. 1992, in preparation

Wood, D.O.S, Myers, P.C., & Daugherty, D. A. 1992, *ApJ*, in preparation

Zuckerman, B., & Palmer, P. 1974, *ARA&A*, **12**, 279

Zweibel, E. G., & Josafatsson, K. 1983, *ApJ*, **270**, 511

FIGURE CAPTIONS

Figure 1. The density profile of linear magnetoacoustic waves in a magnetically supported slab, where neutrals and ions are perfectly coupled. The sound and Alfvén speeds of the fluid are $a_s = 0.1$ km s^{-1} and $v_\alpha = 1.0$ km s^{-1}, respectively. The perturbation velocity is characterized by $v_{10}/v_\alpha = 0.1$, and the wave phase ϕ is determined by applying the boundary condition $\rho_1|_{\xi=0,t=0} = 0$. The solid curve corresponds to $kR = 3$; the short-dashed curve corresponds to $kR = 6$; and the long-dashed curve corresponds to $kR = 10$.

Figure 2. The parameter $\eta \equiv |\rho_{1;\tilde{\gamma}}|/|\rho_{1;0}|$ as a function of ξ, where $\rho_{1;\tilde{\gamma}}$ is the part of the wave density due to the first order $\tilde{\gamma}^{-1}$ corrections, and $\rho_{1;0}$ is the wave density in the absence of the corrections. The solid curve corresponds to $kR = 3$; the short-dashed curve corresponds to $kR = 6$; and the long-dashed curve corresponds to $kR = 10$.

Figure 3. The dashed curve corresponds to the density profile for the same case as was presented in Figure 1a, but with first order $\tilde{\gamma}$ corrections included (for $kR = 3$). For the purpose of comparison, the solution from Figure 1a is also included and represented by the solid curve; the dotted curves correspond to the amplitude of this density profile.

Figure 4. The time-averaged second-order density profile (in arbitrary units) resulting from magnetoacoustic wave propagation in a magnetically supported slab.

Figure 5. The magnetic field strength profile for linear Alfvén waves in a thermally supported slab. The sound and Alfvén speeds of the fluid are $a_s = 0.2$ km s^{-1} and $v_\alpha|_{\xi=2} = 1.0$ km s^{-1}, respectively. The wave phase ϕ is determined by applying the boundary condition $\rho_1|_{\xi=0,t=0} = 0$. The two curves correspond to the following cases: (a) $KR = 6$ ($\tilde{\gamma} = 7.5$); and (b) $KR = 10$ ($\tilde{\gamma} = 4.5$).

Figure 6. Same as Figure 5, but in the artificial limit that $\tilde{\gamma} \to \infty$.

Figure 7. The full time-averaged density profile (up to second order) resulting from Alfvén wave propagation in a thermally supported slab. The solid curve represents the unperturbed state. The dashed curves correspond to the density profiles for the following cases: (a) $(B_{1x0}/B_0)(v_\alpha^2|_{\xi=0}/4a_s^2) = 0.1$; (b) $(B_{1x0}/B_0)(v_\alpha^2|_{\xi=0}/4a_s^2) = 0.25$; (c) $(B_{1x0}/B_0)(v_\alpha^2|_{\xi=0}/4a_s^2) = 0.5$.

Fig. 1

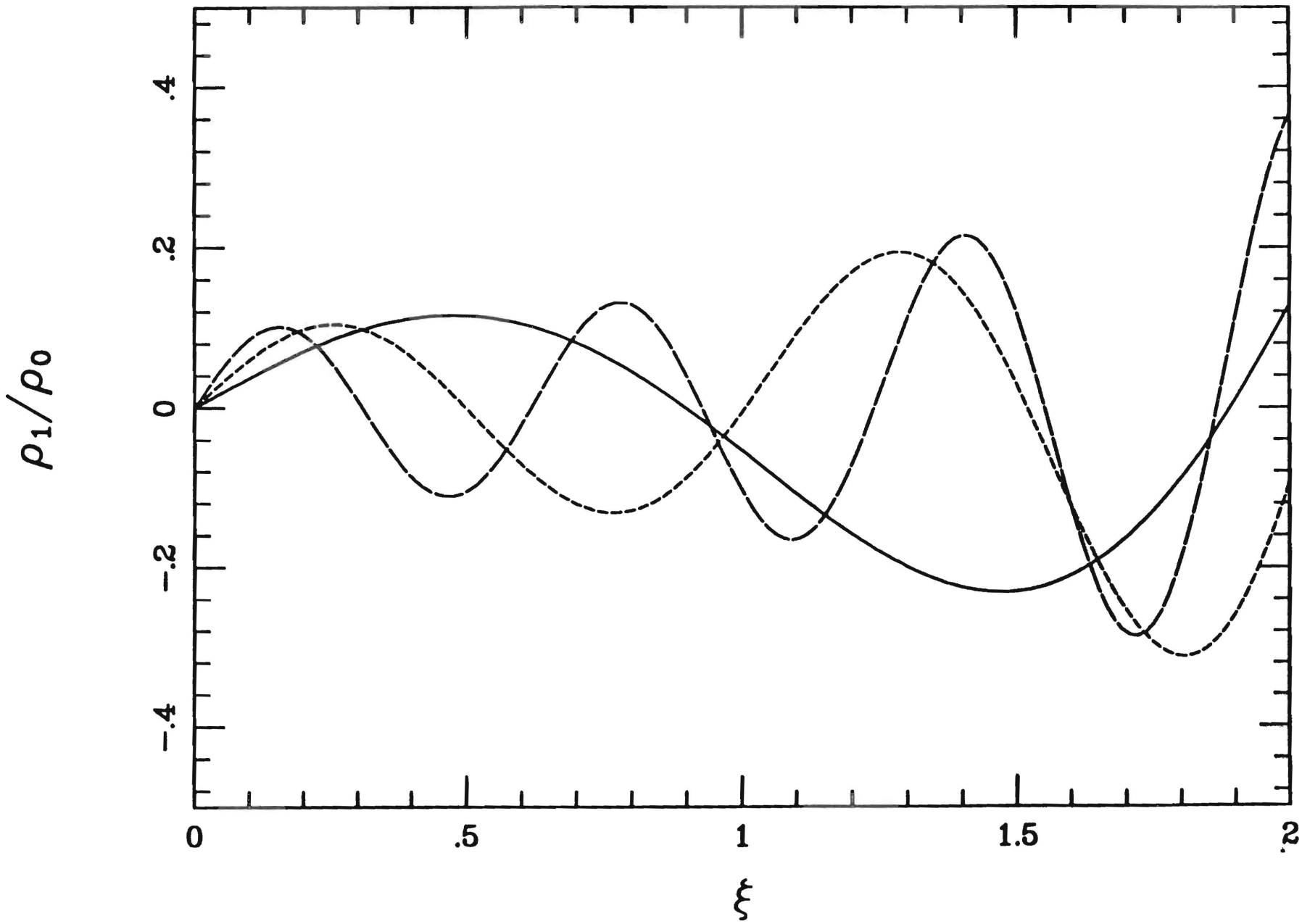

Fig. 2

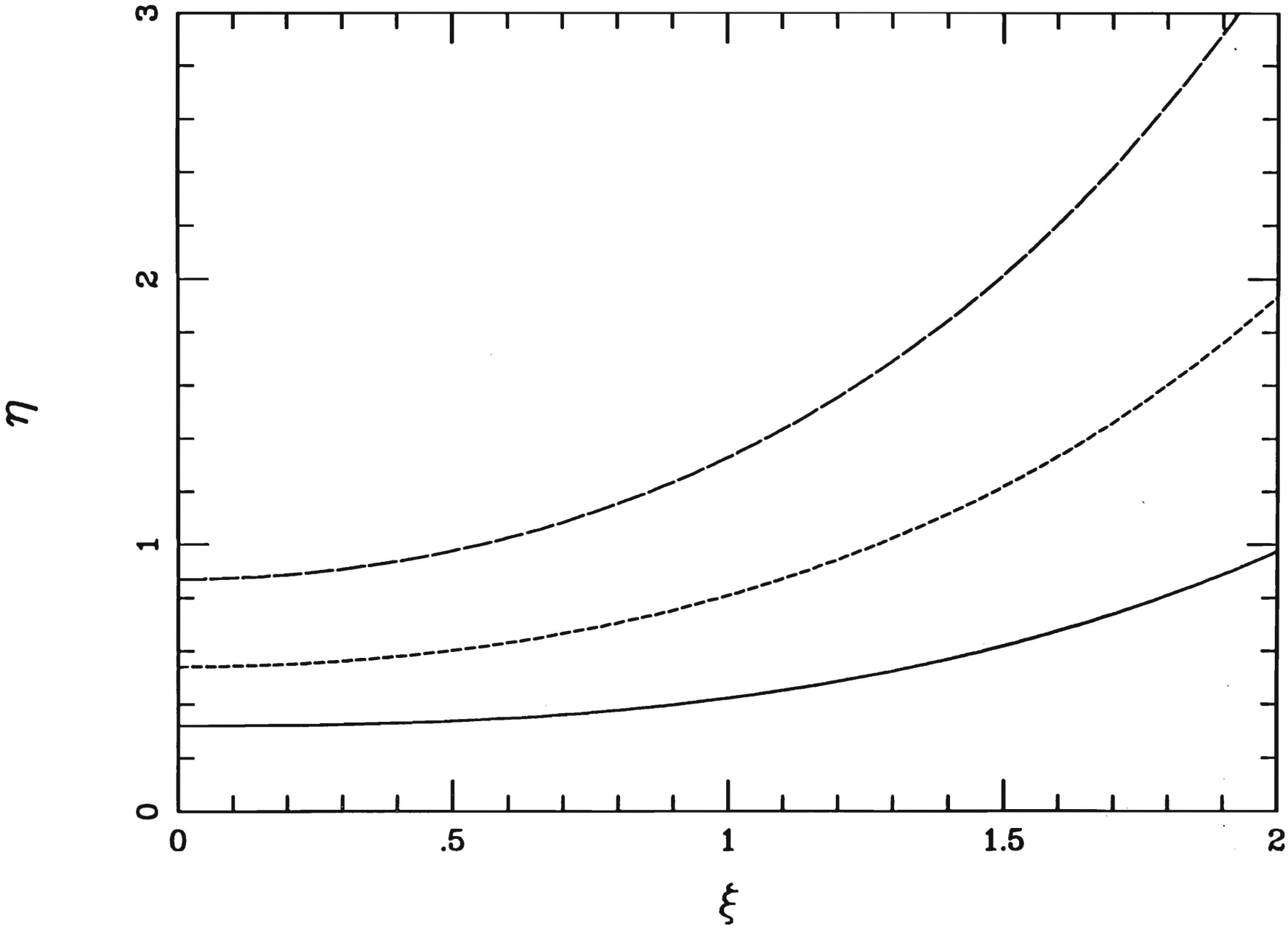

Fig. 3

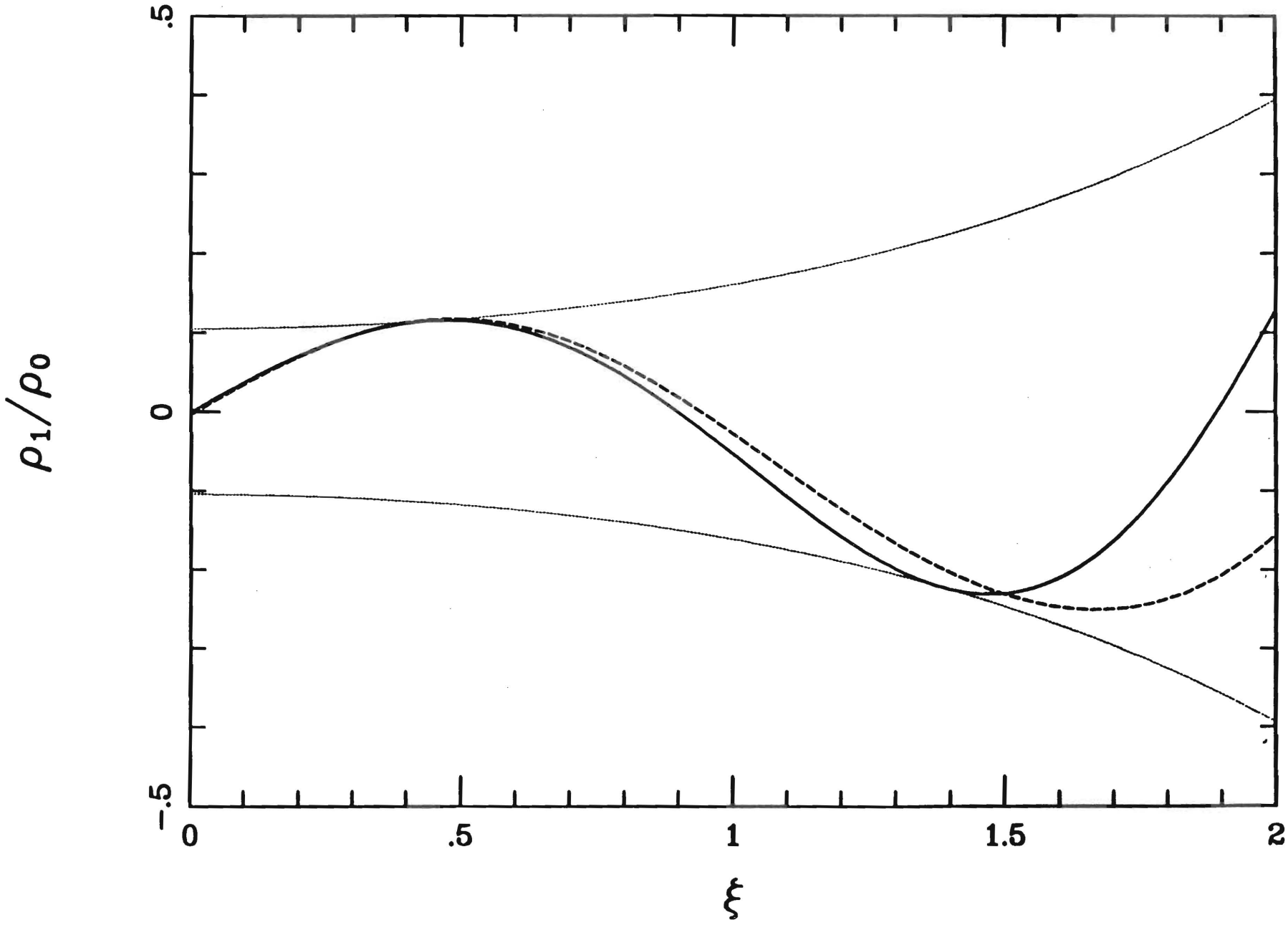

Fig. 4

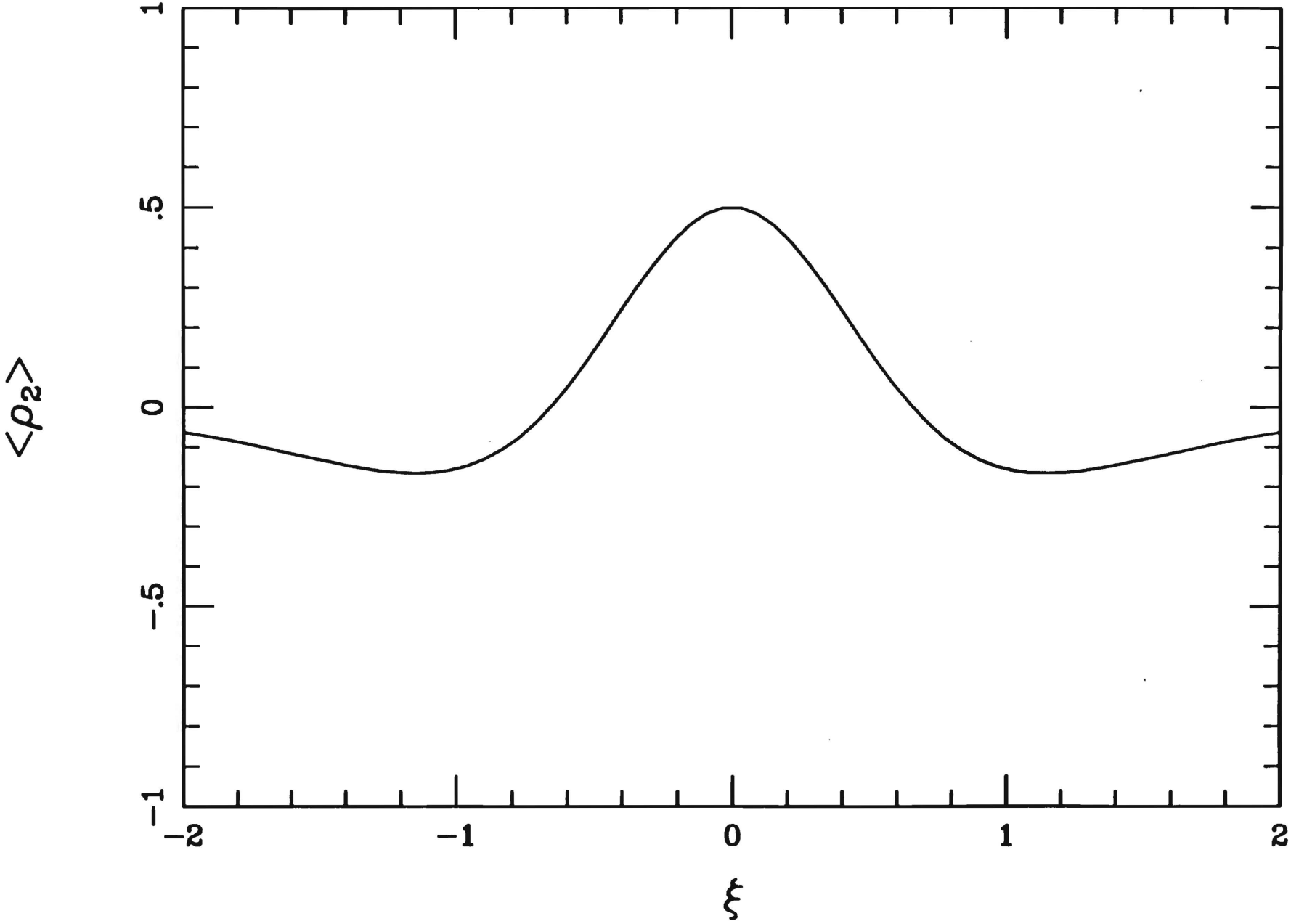

Fig. 5

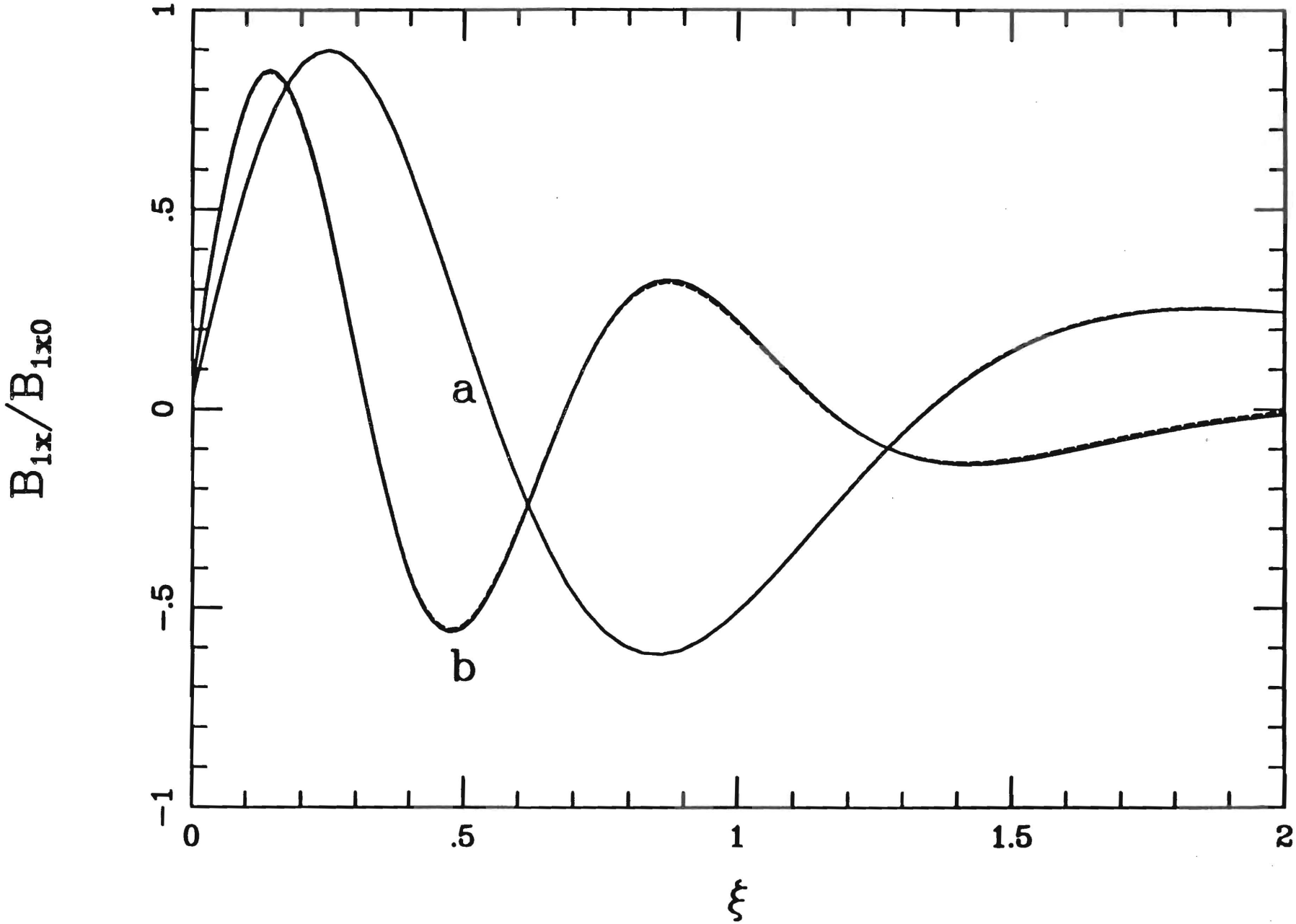

Fig. 6

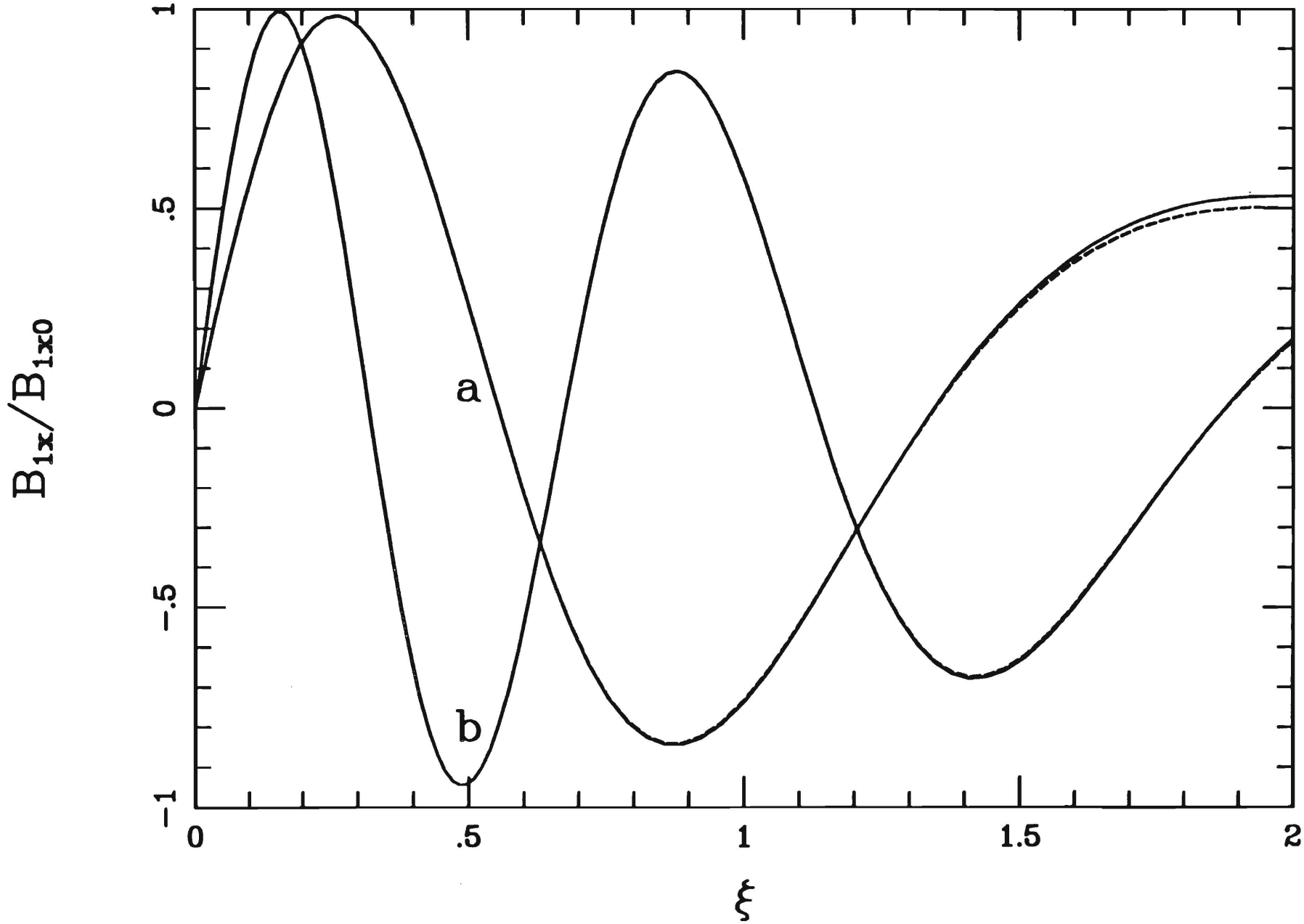
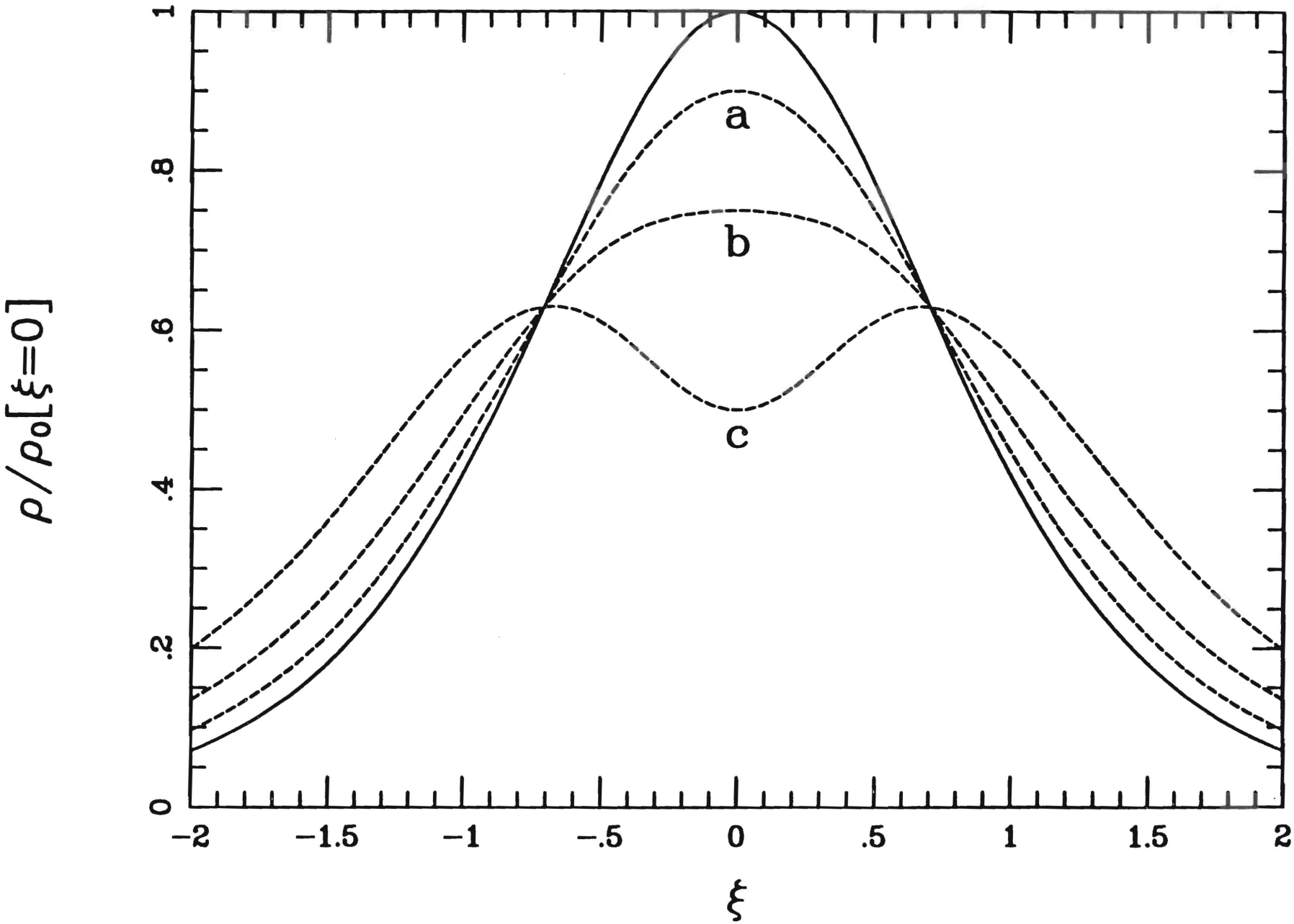
Fig. 7